Inorganic Chemistry

Article

pubs.acs.org/IC

LuF[SeO_3]: The Structural Chameleon of Lanthanoid Fluoride Oxoselenates(IV)

Christian Lipp,[†] Robert E. Dinnebier,[‡] and Thomas Schleid*[,†]

[†]Institute for Inorganic Chemistry, University of Stuttgart, Pfaffenwaldring 55, D-70569 Stuttgart, Germany

[‡]Max Planck Institute for Solid State Research, Heisenbergstrasse 1, D-70569 Stuttgart, Germany

ABSTRACT: LuF[SeO_3] is a compound that can easily be obtained by a solid-state reaction of Lu_2O_3, LuF_3, and SeO_2 with CsBr as the fluxing agent. The outstanding property of LuF[SeO_3] is the appearance of two phase transitions within a range of less than 200 K. With an increase in the coordination number for Lu^{3+} from 7 to 8, the triclinic room-temperature modification changes at temperatures below −40 °C to the monoclinic low-temperature or high-pressure phase of LuF[SeO_3]. At the same time, room-temperature modification retains the structure but gains higher symmetry at the second phase transition of around +110 °C. This second transition can even be observed under a microscope using polarized light to see twinning lamellae disappear and reappear during this reversible process.

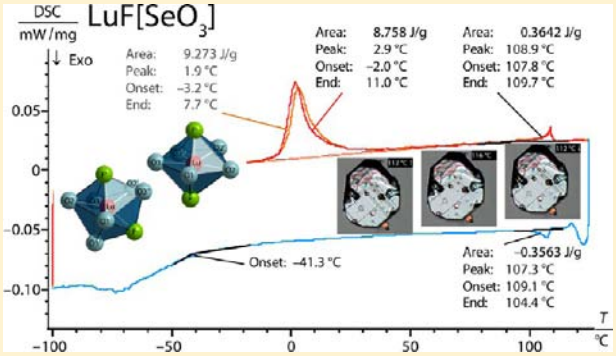

INTRODUCTION

In the search for energy-saving technologies, lanthanoid elements are focused upon for the development of new luminescent materials. This is due to their f−f or f−d transitions,[1] which are of enormous interest for these applications.[2] Host lattices can be formed by rare-earth metal compounds as well. Older examples are Y_2O_3:Eu^{3+} or Y_2O_2S:Eu^{3+}.[3] An advantage of these lattices is the identical charge of the cations while having the flexibility of different ionic radii that are fit to the respective doping agent. In that way, host lattices for the larger lanthanoids might be built up by lanthanum, whereas for the smaller ones (lanthanoid contraction), yttrium or even lutetium might be chosen. We focused our research on rare-earth metal(III) oxoselenates(IV), introducing F^- as a hard anion. The ψ^1-tetrahedral $[SeO_3]^{2-}$ anions with stereochemically active lone pairs at the Se^{4+} centers might serve with s−p transitions as well as with the formation of non-centrosymmetric structures that are necessary for usage in nonlinear optics.

A first member of the formula type MF[SeO_3] (with M = rare-earth metal) was presented by Wickleder for M = La [coordination number (CN) = 10 and 11].[4] So far, we could extend the structure type of LaF[SeO_3] only to cerium, where the crystals appeared at very poor quality. Instead, we obtained the same formula type, but with different structures (CN = 7 or 8), at high yield and quality for M = Y and Ho−Lu.[5−8] Fluoride oxoselenates(IV) of the intermediate lanthanoids appear only with lower fluoride content within the formula type M_3F[SeO_3]$_4$,[9−12] however.

For yttrium (including M = Ho−Yb) and lutetium, we found two different structure types at room temperature with CN = 8 for the YF[SeO_3]-type compounds and CN = 7 for LuF[SeO_3]. Upon cooling of LuF[SeO_3], Lu^{3+} gains a higher CN and the YF[SeO_3]-type structure appears.[8] Additionally, triclinic room-temperature LuF[SeO_3] shows only slight deviations from a higher-symmetric monoclinic structure. Indeed, this assumed second-phase transition could be confirmed by X-ray diffractometry, by differential scanning calorimetry (DSC) measurements, and even optically. These results, including the crystal structure of the new high-temperature phase of LuF[SeO_3] and a comparison with the other two structure types, will be presented in the following, putting an emphasis on the structural changes during both phase transitions.

EXPERIMENTAL SECTION

Evacuated silica ampules were used for the synthesis of LuF[SeO_3]. By reaction of fluorides in silica ampules, the formation of silicates has to be expected. Therefore, the fused silica has to be thoroughly heated before usage to heal any damages on the surface. Second, acetone has to be brought to decomposition inside the ampules without the presence of oxygen in order to seal and protect the inner wall with a layer of carbon. Taking these precautions into account, all MF[SeO_3] compounds can be easily obtained at high yield in fused silica ampules, which is an elegant way of avoiding the costly usage of coinage metal ampules.

A total of 100.0 mg of lutetium sesquioxide (Lu_2O_3; ChemPur, 99.9%), 62.0 mg of lutetium trifluoride (LuF_3; ChemPur, 99.9%), and 147.4 mg of selenium dioxide (SeO_2; Acros, 99.8%) in a molar ratio of 1:1:3 were mixed for the synthesis of LuF[SeO_3] with a surplus of CsBr (E. Merck, suprapur) as the fluxing agent, and reaction took place for 5 days at 750 °C. After the ampules were opened, CsBr was dissolved and removed with the help of demineralized water. Single crystals without signs of twinning were then taken for the

Received: March 14, 2013
Published: September 11, 2013

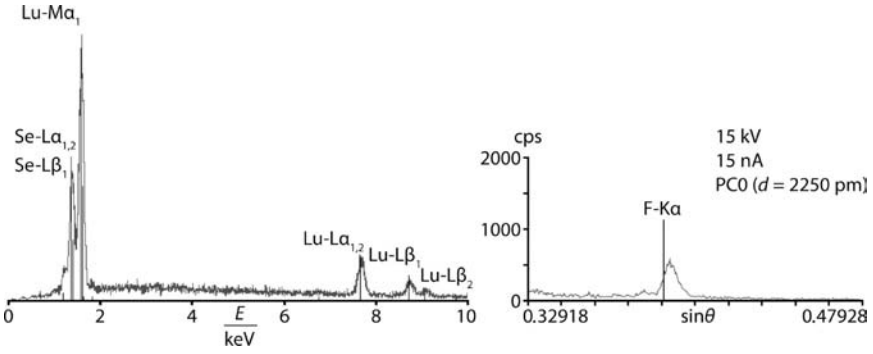

Figure 1. Verification of the incorporated elements with the help of an electron microprobe (Cameca SX100): left, EDS spectrum; right, fluorine as detected with one of the WDS spectrometers.

Table 1. Crystallographic Data for the Three Phases of $LuF[SeO_3]$ and Their Determination[a]

	LT $LuF[SeO_3]$ at −173 °C	RT $LuF[SeO_3]$ at +25 °C	HT $LuF[SeO_3]$ at +150 °C
crystal system	monoclinic	triclinic	monoclinic
space group	$P2_1/c$ (no. 14)	$P\bar{1}$ (no. 2)	$P2_1/m$ (no. 11)
lattice parameters			
a (pm)	648.39(6)	644.85(6)	647.34(5)
b (pm)	681.28(7)	684.41(7)	687.02(6)
c (pm)	705.81(7)	427.98(4)	428.43(4)
α (deg)	90	94.063(5)	90
β (deg)	98.657(5)	96.484(5)	95.602(5)
γ (deg)	90	91.895(5)	90
cell volume V (nm^3)	0.30823(5)	0.18704(3)	0.18963(3)
number of formula units Z	4	2	2
calculated density D_x (g cm^{-3})	6.916	5.698	5.621
molar volume V_m (cm^3 mol^{-1})	46.405	56.318	57.094
index range ($\pm h_{max}$, $\pm k_{max}$, $\pm l_{max}$)	9, 9, 9	8, 9, 5	6, 8, 5
$2\theta_{max}$ (deg)	56.7	56.6	54.9
$F(000)$	552	276	276
absorption coefficient μ (mm^{-1})	43.68	35.99	35.50
observed reflections	8342	6683	1693
unique reflections	771	925	417
R_{int}/R_σ	0.092/0.051	0.060/0.027	0.065/0.040
reflections with $\lvert F_o\rvert \geq 4\sigma(F_o)$	721	889	400
R1/R1 with $\lvert F_o\rvert \geq 4\sigma(F_o)$	0.038/0.035	0.023/0.021	0.029/0.028
wR2/GOF	0.083/1.060	0.051/1.066	0.061/1.054
extinction g	0.0119(9)	0.0302(15)	0.0031(9)
residual electron densities $\Delta\rho_{max/min}$ (e^- 10^{-6} pm^{-3})	2.11/−1.94	1.90/−1.24	2.16/−1.57
ICSD number	419588	417449	424605

[a]Instrument: κ-CCD (Bruker-Nonius). Wavelength: Mo Kα (λ = 71.07 pm). Monochromator: graphite. Data corrections: programs *X-RED* and *X-SHAPE*.[33] Structure determination and refinement: program package *SHELX-97*.[34] Scattering factors: *International Tables*, Vol. C[35]).

measurements (−173 °C, room temperature, and 150 °C) at a κ-CCD single-crystal X-ray diffractometer (Bruker-Nonius). The successful incorporation of fluorine was examined with the help of a Cameca SX100 electron microprobe (Figure 1).

Powder X-ray diffraction data of $LuF[SeO_3]$ were collected at low temperature with a Stoe Stadi-P laboratory diffractometer in Debye–Scherrer geometry (primary beam Johannson-type Ge(111) monochromator for Cu Kα_1 radiation and a linear position-sensitive detector, PSD) using an Oxford Cryostream 700 cold-air blower with the sample sealed in a borosilicate glass capillary of 0.3 mm diameter. The powder patterns of $LuF[SeO_3]$ were recorded with dependence on the temperature from room temperature to 110 K in steps of 5 or 10 K in the range from 2θ = 5 to 60° with a step width of 2θ = 0.01° using a linear PSD with an opening of approximately 2θ = 12°.

Powder diffraction data for $LuF[SeO_3]$ at high temperature were collected with the high-resolution powder diffractometer I11 at Diamond, Great Britain.[13−15] The wavelength was determined to be 0.8264(3) Å from a silicon standard. The sample was contained in a sealed 0.1 mm quartz capillary. The diffracted beam was detected with a series of Mythen PSDs with 90° aperture. The sample was heated from room temperature to 300 °C at 3 K/min. Powder patterns were collected continuously for 14 s/frame. All samples were rotated around θ in order to improve randomization of the crystallites.

The peak profiles and precise lattice parameters for all three phases were determined by Le Bail fits[16] using the fundamental parameter approach,[17] as implemented in *TOPAS*, version 4.1 (Bruker-AXS).

Additionally, the phase transitions were studied by DSC, using a DSC-204 Phoenix or a F1 device (Netzsch), and the high-temperature phase transition was documented via a TS1500 heating stage (Linkam) that was mounted on an Olympus BX51 research microscope.

RESULTS AND DISCUSSION

$LuF[SeO_3]$ appears at *room temperature* (RT) triclinically with space group $P\bar{1}$ (no. 2), a = 644.85(6) pm, b = 684.41(7) pm, c = 427.98(4) pm, α = 94.063(5)°, β = 96.484(5)°, γ =

dx.doi.org/10.1021/ic4006289 | *Inorg. Chem.* 2013, 52, 10788−10794

91.895(5)°, and Z = 2. Moving to the *high-temperature* (HT) phase, these cell dimensions change only slightly. At 150 °C, the HT phase shows monoclinic symmetry with the space group $P2_1/m$ (no. 11) and a = 647.34(5) pm, b = 687.02(6) pm, c = 428.43(4) pm, β = 95.602(5)°, and Z = 2. In the *low-temperature* (LT; alternatively, HP for *high-pressure* might also be used) phase, $LuF[SeO_3]$ crystallizes monoclinically again, but now with space group $P2_1/c$ (no. 14) and a = 648.39(6) pm, b = 681.28(7) pm, c = 705.81(7) pm, β = 98.657(5)°, and Z = 4 (further details to the single-crystal X-ray diffractometry can be taken from Table 1). Because the cell dimensions of the RT and HT phases are quite similar, the same is therefore observed for the molar volumes with V_m(RT) = 56.318 cm^3/mol and V_m(HT) = 57.099 cm^3/mol, opposing that the phase transition from the RT phase to the LT (or HP) phase shows a drastic change, however. While the number of formula units doubles, the c axis remains much shorter than necessary for a similar cell volume. Thus, it is not surprising that the molar volume drops to only V_m(LT/HP) = 46.405 cm^3/mol, which is accompanied by an increase of the calculated density from 5.698 to 6.916 g/cm^3 (+21.4%). With the apparent possibility of a HT phase transition, a DSC measurement was carried out in order to determine the exact temperatures of both phase transitions (Figure 2).

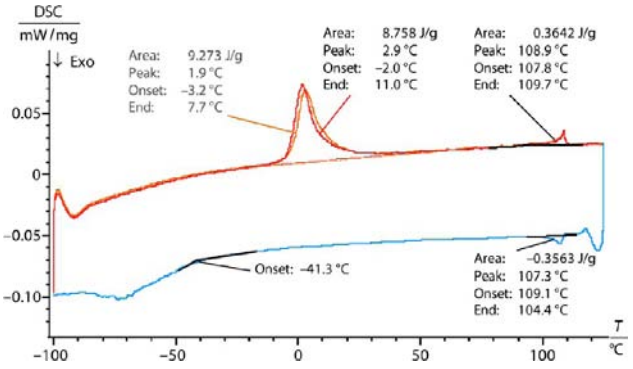

Figure 2. DSC data (Netzsch DSC-204 F1) showing the phase transitions of $LuF[SeO_3]$ (heating and cooling rate of 5 K min^{-1}).

At RT and HT, Lu^{3+} is surrounded by five equatorial O^{2-} and two apical F^- anions in the shape of a pentagonal bipyramid $[LuO_5F_2]^{9-}$ (Figure 3). An identical arrangement can be found at the closely related $CsTmCl_2[SeO_3]$-type structures[18,19] but surprisingly not for the formula-type $MCl[SeO_3]$[20−22] with $HoCl[TeO_3]$-analogous structure,[23] where one of the two Cl^- anions appears in the equatorial plane. Like in $CsTmCl_2[SeO_3]$,[18] pentagonal bipyramids $[LuO_5F_2]^{9-}$ are sharing trans-oriented edges along [010] to form $^1_\infty\{[LuO^e_{4/2}O^t_{1/1}F^t_{2/1}]^{5-}\}$ strands (e = edge sharing and t = terminal; see Figure 4). These chains are then consecutively connected to each other via the apical F^- anions, generating $^2_\infty\{[Lu(O3)_{2/2}(O2)_{2/2}(O1)_{1/1}F_{2/2}]^{4-}\}$ sheets parallel to the (100) plane. Charge balance is finally achieved by the Se^{4+} cations, which are connected to all of the O^{2-} anions, forming ψ^1-tetrahedral $[SeO_3]^{2-}$ groups. The analogy to $CsTmCl_2[SeO_3]$ becomes more apparent when sheets parallel to (001) are described by connecting the $^1_\infty\{[LuO^e_{4/2}O^t_{1/1}F^t_{2/1}]^{5-}\}$ strands with the Se^{4+} cations (Figure 4). The resulting $^2_\infty\{(LuF_2[SeO_3])^-\}$ sheets are apparently identical with those ($^2_\infty\{(TmCl_2[SeO_3])^-\}$) in $CsTmCl_2[SeO_3]$. More precisely, this structural motif can

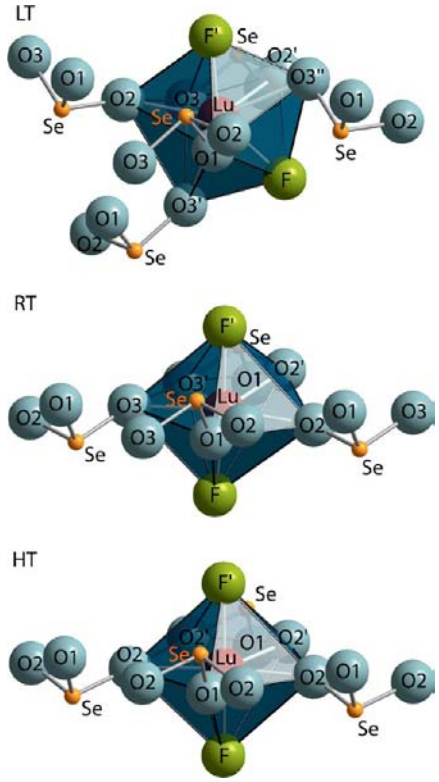

Figure 3. Coordinative environment of the Lu^{3+} cations and the adjacent ψ^1-tetrahedral $[SeO_3]^{2-}$ units in the three phases of $LuF[SeO_3]$.

also be found in *α-uranophane* ($Ca([UO_2][SiO_3OH])_2{\cdot}5H_2O$) as described by Burns et al.[24] What is found there as a $^2_\infty\{([UO_2][SiO_3OH])^-\}$ sheet can be presented here as a $^2_\infty\{(LuF_2[SeO_3E])^-\}$ layer when electron lone pairs E are introduced as fourth ligands to the Se^{4+} cations. Even the orientation of the $[SiO_3(OH)]^{3-}$ and $[SeO_3E]^{2-}$ tetrahedra appears in the same up, down, up, down sequence (UDUD; Burns et al.[24]). Because the structure of LT $LuF[SeO_3]$ with $YF[SeO_3]$-type structure can be deduced from the RT phase, a detailed description will not follow at this point in order to avoid redundancies. The important aspects be shown with explanations of the phase transitions.

Prior to this, a short glance at some important distances and angles should be given. The distances d(Lu−O) within the pentagonal bipyramids appear at RT in a range of 223−236 pm and very similar (222−234 pm) at 150 °C (see Table 2 for details). As Lu^{3+} gains a higher CN with the LT phase, these values have to increase to 225−239 and *258* pm. Also, no significant differences can be found for d(Lu−F), where the RT phase shows 214 and 215 pm, whereas 213 and 215 pm are found for the HT phase and about 216 pm each for LT $Lu[SeO_3]$. Taking the smaller CN of 6 in C-type Lu_2O_3[25] into account, comparable distances Lu−O of 218−228 pm can be reported there. The Lu−F distances might be compared with those in LuF_3, which is isotypic to YF_3.[26−28] Accompanied by the higher CN of 8 + *1*, values of 220−228 and *263* pm can be found. This interval increases even further within $Lu_3O_2F_5$[29] [CN(Lu^{3+}) = 7 + *1* and 8: d(Lu−F) = 216−245 pm + *278* pm].

The ψ^1-tetrahedral $[SeO_3]^{2-}$ anions are not affected very much by both phase transitions. At LT, the Se−O bond lengths amount to 168, 172, and 174 pm, which slightly decrease to 166, 171, and 172 pm at RT and finally to 166 and 171 pm

dx.doi.org/10.1021/ic4006289 | Inorg. Chem. 2013, 52, 10788−10794

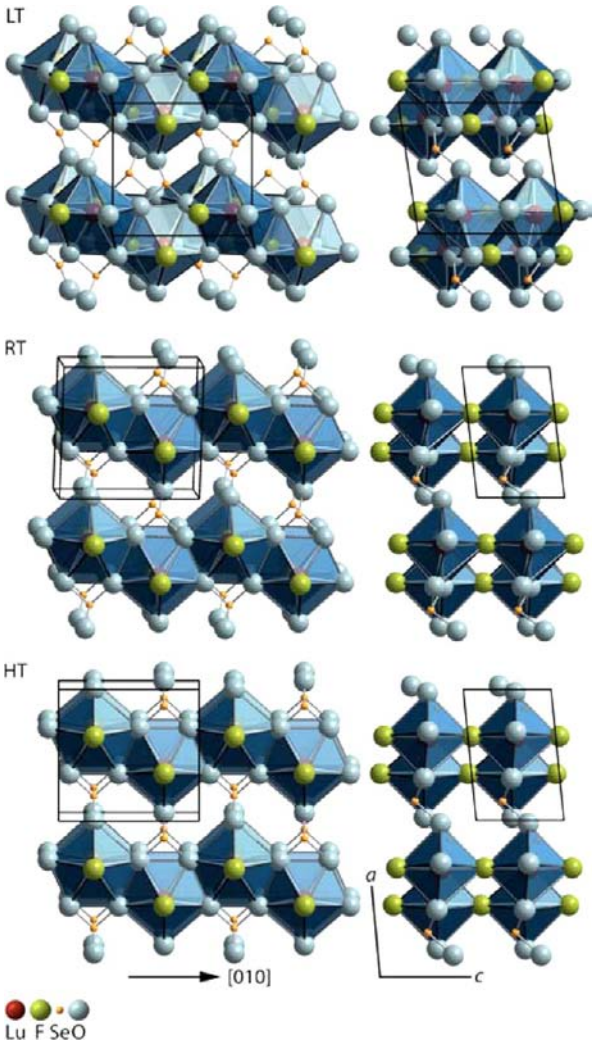

Figure 4. Comparison of the three modifications of $LuF[SeO_3]$. Please note that the left column represents views onto the (001) plane, while the right column represents views along [0$\bar{1}$0]. The RT phase loses the mirror planes of the HT phase by a slight change of the angles α and γ from 90° to about 94.1° and 91.9°, respectively.

(2×) within the HT phase. The angles ∠(O−Se−O) are 2 times in a range of 103−104°, while the third one in the $[SeO_3]^{2-}$ units decreases from 92° (LT phase) via 91° at RT to about 90° for HT $LuF[SeO_3]$ (detailed values for the $[SeO_3]^{2-}$ anions are presented in Table 2).

While the appearance of the LT phase might be a bit surprising at first glance, the phase transition to the HT phase follows the apparent possibility to gain a higher symmetry by accomplishing only a minor structural change. The isolated ψ^1-tetrahedral $[SeO_3]^{2-}$ anions differ only slightly from 2-fold symmetry in the triclinic RT phase and the necessary change is accomplished by attainment of temperatures of about 110 °C, where the Se−O1 bond slightly turns, finally residing on a mirror plane with an orientation perpendicular to [010]. Besides Se and O1, also Lu and F reside within the same mirror plane (Figure 4). This is accompanied by an overall increase of the structural symmetry, resulting in the monoclinic space group $P2_1/m$ (no. 11), which represents a minimal non-isomorphic supergroup to the triclinic space group $P\bar{1}$ (no. 2). Thus, this transition is translationengleich with index 2 (Figure 5).

Table 2. Selected Interatomic Distances (d/pm) and Angles (∠/deg) for the Three Phases of $LuF[SeO_3]$

	−173 °C/LT	+25 °C/RT	+150 °C/HT
Lu−O1	224.6(6)	223.4(4)	222.2(8)
Lu−O2	231.3(6)	223.1(3)	224.9(5) (2×)
Lu−O2′	235.2(6)	236.3(4)	234.0(6) (2×)
Lu−O3	237.9(6)	226.0(3)	
Lu−O3′	238.5(6)	233.3(4)	
Lu−O3″	258.0(6)		
Lu−F	216.0(5)	214.2(3)	213.3(6)
Lu−F′	216.2(6)	214.6(3)	215.4(6)
Se−O1	167.7(6)	165.7(4)	166.2(8)
Se−O2	172.0(6)	171.0(3)	171.0(6) (2×)
Se−O3	173.8(6)	171.9(4)	
Se···(O1,O2,O3)	80.1	79.8	
Se···(O1,O2,O2)			80.1
O2−Se−O2			89.7(4)
O2−Se−O3	91.7(3)	90.6(2)	
O1−Se−O3	103.2(3)	103.9(2)	
O1−Se−O2	104.1(3)	103.6(2)	103.9(3) (2×)
F−Lu−F′	133.2(2)	172.9(2)	176.4(4)
Lu−F−Lu′	125.0(2)	172.9(2)	176.4(4)

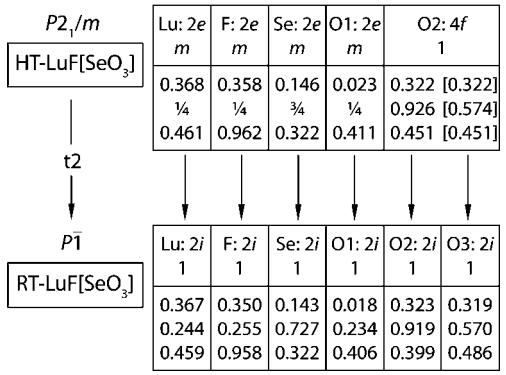

Figure 5. Phase transition of $LuF[SeO_3]$ between the RT and HT phases appearing as translationengleich with index 2.

Under polarized light, some of the crystals show twin lamellae at RT that are a result of this phase transition. We could confirm this assumption by bringing a twinned crystal on a hot stage and observing the crystal under polarized light, while repeatedly running a heating and cooling program. Upon attainment of the transition temperature, the twin lamellae will disappear and reappear with each cycle exactly as expected (Figure 6).

As mentioned above, the density increases from 5.698 to 6.916 g/cm^3 while $LuF[SeO_3]$ changes below −40 °C to the monoclinic $YF[SeO_3]$-type structure as the LT phase. This is a drastic change of +21.4% that is achieved by contraction of the structure along [001] (Figures 4 and 7). A short glance at the lattice parameters of both phases indicates this fact already quite well. While both the a and b axes remain at virtually the same values, the c axis increases from about 428 pm to only 706 pm, whereas the number of formula units doubles from 2 to 4. At the same time, it is helpful to follow the structural change along [001] by reducing the structure of $LuF[SeO_3]$ to only its Lu^{3+} and F^- anions. Only $^1_\infty\{[LuF^v_{2/2}]^{2+}\}$ strands (v = vertex sharing) with angles of 173° for Lu−F−Lu′ *and* F−Lu−F′ running along [001] remain now. The shortening along the c

dx.doi.org/10.1021/ic4006289 | Inorg. Chem. 2013, 52, 10788−10794

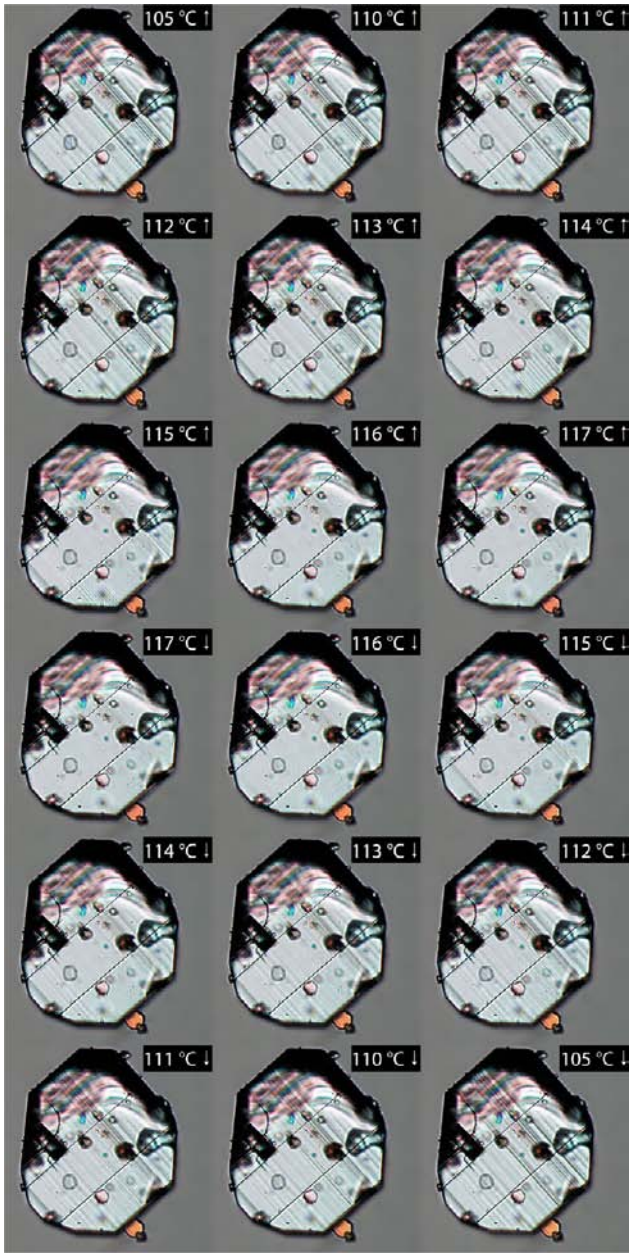

Figure 6. Phase transition of $LuF[SeO_3]$ from the triclinic RT phase to the monoclinic HT phase observed under polarized light with the help of the appearance and disappearance of twin lamellae (two parallel cracks are running perpendicular to the twin lamellae of the shown $LuF[SeO_3]$ crystal; diameter of the crystal: 0.2 mm).

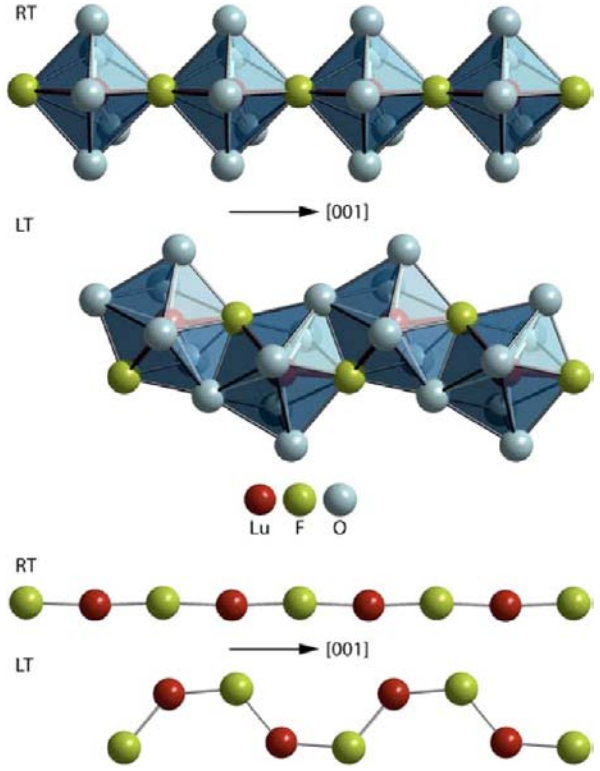

Figure 7. Having reached the monoclinic $YF[SeO_3]$-type structure as the LT phase, contraction along [001] results in a higher CN for Lu^{3+} (CN = 7 → 8) and a much higher density for LT $LuF[SeO_3]$.

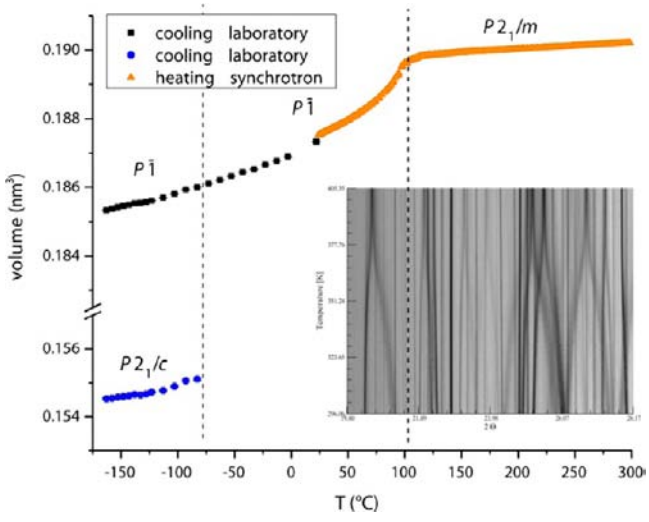

Figure 8. Temperature dependence of the volume of $LuF[SeO_3]$ in the temperature range from −170 to +300 °C showing three different phases (denoted by their different space groups). The inset shows a cut-out of the two-dimensional projection (simulated heating−Guinier pattern prepared using *Powder3D*[32] of the observed scattered X-ray intensity for $LuF[SeO_3]$ around the phase transition from the RT to HT phase as a function of the diffraction angle (x axis) and temperature (y axis; RT → 132 °C at 3 K min^{-1}).

axis changes these values to 125° (Lu−F−Lu′) and 133° (F−Lu−F′), and the $^1_\infty\{[LuF^v_{2/2}]^{2+}\}$ strands appear as zigzag chains (Figure 7).

When all O^{2-} anions are added to this description, simultaneous rotation of the polyhedra brings an $(O3)^{2-}$ anion of a pentagonal bipyramid in contact with the neighboring Lu^{3+} cation, thus changing its CN from 7 to 8. The new $[LuO_6F_2]^{2-}$ polyhedra are therefore no longer connected by only F^- vertices but by O3···O3 and O3···F edges. Hence, the $^2_\infty\{[Lu(O3)_{2/2}(O2)_{2/2}(O1)_{1/1}F_{2/2}]^{4-}\}$ sheets of RT $LuF[SeO_3]$ transform to $^2_\infty\{[Lu(O3)_{3/3}(O2)_{2/2}(O1)_{1/1}F_{2/2}]^{4-}\}$ sheets in LT $LuF[SeO_3]$. Despite this structural change with an increased CN for Lu^{3+}, the similarity between both structures remains remarkably high (Figure 4).

Additionally, the phase transitions as determined from single-crystal data could be confirmed by powder X-ray diffraction (Figure 8). Interestingly, the occurrence of the LT phase transition seems to be kinetically hindered, meaning that it does

dx.doi.org/10.1021/ic4006289 | *Inorg. Chem.* 2013, 52, 10788−10794

either not occur or not quantitatively upon cooling to −170 °C. In the data presented in Figure 8, both phases, RT and LT, coexist upon cooling in the temperature range from −75 to −170 °C.

The nature of the RT−HT phase transition is quite complicated and is the subject of an upcoming paper.[30,31] In general, the order of the phase transition depends upon the thermal history of the sample. Previous cooling of the material without undergoing the RT−LT phase transition creates a substantial amount of strain in the material. In this case, upon heating of $LuF[SeO_3]$, the structural phase transition at 120 °C is close to a second-order phase transition, while upon cooling, the phase transition occurs at 98 °C, showing a large hysteresis typical for a first-order phase transition. Detailed analysis using sequential and parametric whole powder pattern fitting revealed that the coupling between strains and the order parameter determines the behavior of the material during the phase transition. Upon heating, the phase transition occurs at about 120 °C because of the biquadratic coupling between strains and the order parameter. Upon cooling, the phase transition occurs at about 98 °C because of the bilinear coupling between symmetry-breaking strains and the order parameter and linear-quadratic (biquadratic) coupling between nonsymmetry-breaking strains and the order parameter.

CONCLUSIONS AND OUTLOOK

With this study, we are able to present a strictly inorganic compound ($LuF[SeO_3]$) with two phase transitions at very moderate temperatures, where the first one is characterized only by a slight structural change to gain higher symmetry. The second phase transition instead is accompanied by an increasing CN for Lu^{3+} and a higher density. Quite remarkable is that these phase transitions appear in a relatively narrow temperature range. Thus, $LuF[SeO_3]$ can serve as a model for investigations on the material properties, where the direct influence of a lattice is in the focus of research. Especially, the study of the dependence of the luminescence properties after doping with the most suitable M^{3+} cations of the lanthanoids (e.g. Eu^{3+} or Tb^{3+}) will be an interesting task.

AUTHOR INFORMATION

Corresponding Author

*E-mail: schleid@iac.uni-stuttgart.de. Fax: +49(0)711/685-64241.

Notes

The authors declare no competing financial interest.

ACKNOWLEDGMENTS

For capital and staff appropriations, we thank the State of Baden-Württemberg (Stuttgart, Germany), the Fonds der Chemischen Industrie (Frankfurt/Main, Germany), and the Deutsche Forschungsgemeinschaft (Bonn, Germany) in the course of the priority program SPP 1166 ("Lanthanoidspezifische Funktionalitäten in Molekül und Material"/"Lanthanoid-specific Functionalities in Molecules and Materials"). For data collection at the κ-CCD single-crystal diffractometer, we are indebted to Dr. Ingo Hartenbach and Dr. Falk Lissner. For the DSC measurements, we thank CTA Christof Schneck and Prof. Dr. Anja-Verena Mudring (Ruhr University Bochum, Bochum, Germany).

REFERENCES

(1) Binnemans, K. *Chem. Rev.* **2009**, *109*, 4283−4374.
(2) Bünzli, J.-C. G.; Piguet, C. *Chem. Soc. Rev.* **2005**, *34*, 1048−1077. Eliseeva, S. V.; Bünzli, J.-C. G. *New J. Chem.* **2011**, *35*, 1165−1176.
(3) Jüstel, Th.; Nikol, H.; Ronda, C. *Angew. Chem., Int. Ed.* **1998**, *37*, 3084−3103.
(4) Wickleder, M. S. *Z. Anorg. Allg. Chem.* **2000**, *626*, 547−551.
(5) Lipp, C.; Schleid, Th. *Z. Anorg. Allg. Chem.* **2007**, *633*, 1429−1434.
(6) Lipp, C.; Schleid, Th. *Z. Anorg. Allg. Chem.* **2008**, *634*, 657−661.
(7) Lipp, C.; Schleid, Th. *Z. Anorg. Allg. Chem.* **2008**, *634*, 1662−1668.
(8) Lipp, C.; Schleid, Th. *Z. Naturforsch.* **2009**, *64 b*, 375−382.
(9) Wickleder, M. S.; Göhausen, I. *Z. Anorg. Allg. Chem.* **2000**, *626*, 1725−1727.
(10) Krügermann, I.; Wickleder, M. S. *J. Solid State Chem.* **2002**, *167*, 113−118.
(11) Krügermann, I. Dissertation, Universität Köln, Köln, Germany, 2002.
(12) Lipp, C. Dissertation, Universität Stuttgart, Stuttgart, Germany, 2008.
(13) Parker, J. E.; Thompson, S. P.; Cobb, T. M.; Yuan, F.; Potter, J.; Lennie, A. R.; Alexander, S.; Tighe, C. J.; Darr, J. A.; Cockcroft, J. C.; Tang, C. C. *J. Appl. Crystallogr.* **2011**, *44*, 102−110.
(14) Thompson, S. P.; Parker, J. E.; Potter, J.; Hill, T. P.; Birt, A.; Cobb, T. M.; Yuan, F.; Tang, C. C. *Rev. Sci. Instrum.* **2009**, *80*, 075107.
(15) Thompson, S. P.; Parker, J. E.; Marchal, J.; Potter, J.; Birt, A.; Yuan, F.; Fearn, R. D.; Lennie, A. R.; Street, S. R.; Tang, C. C. *J. Synchrotron Radiat.* **2011**, *18*, 637−648.
(16) Le Bail, A.; Duroy, H.; Fourquet, J. L. *Mater. Res. Bull.* **1988**, *23*, 447−452.
(17) Cheary, R. W.; Coelho, A. A.; Cline, J. P. *J. Res. Natl. Inst. Stand. Technol.* **2005**, *109*, 1−25.
(18) Wontcheu, J. Dissertation, Universität Stuttgart, Stuttgart, Germany, 2004.
(19) Wickleder, M. S. In *Handbook on the Physics and Chemistry of Rare Earths*; Gschneidner, K. A., Bünzli, J.-C. G., Pecharsky, V. K., Eds.; Elsevier: Amsterdam, The Netherlands, 2005.
(20) Wickleder, M. S. *Z. Naturforsch.* **2002**, *57 b*, 1414−1418.
(21) Berdonosov, P. S.; Shabalin, D. G.; Olenev, A. V.; Demianets, L. N.; Dolgikh, V. A.; Popovkin, B. A. *J. Solid State Chem.* **2003**, *174*, 111−115.
(22) Wickleder, M. S. *Acta Crystallogr.* **2003**, *E 59*, i31−i32.
(23) Meier, S. F.; Schleid, Th. *Z. Anorg. Allg. Chem.* **2002**, *628*, 526−528.
(24) Burns, P. C.; Miller, M. L.; Ewing, R. C. *Can. Mineral.* **1996**, *34*, 845−880.
(25) Hanic, F.; Hartmanová, M.; Knab, G. G.; Urusovskaya, A. A.; Bagdasarov, K. S. *Acta Crystallogr.* **1984**, *B 40*, 76−82.
(26) Zalkin, A.; Templeton, D. H. *J. Am. Chem. Soc.* **1953**, *75*, 2453−2458.
(27) Bukvetskii, B. V.; Garashina, L. S. *Russ. J. Coord. Chem.* **1977**, *3*, 1024−1028.
(28) Greis, O.; Petzel, T. *Z. Anorg. Allg. Chem.* **1974**, *403*, 1−22.
(29) Laval, J. P.; Taoudi, A.; Abaouz, A.; Frit, B. *J. Solid State Chem.* **1995**, *119*, 125−130.
(30) Magdysyuk, O. V.; Dinnebier, R. E.; Lipp, C.; Schleid, Th. *Z. Kristallogr.* **2013**, *Suppl. 33*, 25−25.
(31) Magdysyuk, O. V.; Müller, M.; Dinnebier, R. E.; Lipp, C.; Schleid, Th. *J. Appl. Crystallogr.* **2013**, in press.
(32) Hinrichsen, B.; Dinnebier, R. E.; Jansen, M. *Z. Kristallogr.* **2006**, *23*, 231−236.
(33) Herrendorf, W.; Bärnighausen, H. *HABITUS*: Program for the Optimization of the Crystal Shape for the Numerical Absorption Correction in *X-SHAPE* (version 1.06, Fa. Stoe, Darmstadt, 1999; Karlsruhe, 1993; Gießen, 1996) and *X-RED* (version 1.19, Fa. Stoe, Darmstadt, 1999).
(34) Sheldrick, G. M. *Acta Crystallogr.* **2008**, *A64*, 112−122.

(35) Hahn, Th., Wilson, A. J. C., Eds. *International Tables for Crystallography*; Kluwer Academic Publishers: Dordrecht, The Netherlands, 1992; Vol. C.